PAPER

Check for updates

Removal of atrazine from aqueous solutions onto a magnetite/chitosan/activated carbon composite in a fixed-bed column system: optimization using response surface methodology

Ignace Agani,[a] Jacques K. Fatombi, [ID] *[ab] Sèmiyou A. Osseni, [ID] [a] Esta A. Idohou,[a] David Neumeyer, [ID] [c] Marc Verelst,[c] Robert Mauricot[c] and Taofiki Aminou[b]

In this study, a magnetite/chitosan/activated carbon (MCHAC) composite is proposed as an efficient adsorbent for the removal of atrazine from aqueous solutions. The prepared composite was characterized using Fourier-transform infrared (FTIR) and X-ray diffraction (XRD) methods. Response surface methodology (RSM) coupled with composite central design (CCD) were used to optimize the effects of the four independent variables, pH, initial concentration of atrazine (C_0), bed depth (H), and flow rate (Q), which influence the adsorption process. The experimental results modeled using response surface methodology (RSM) coupled with central composite design (CCD) (RSM–CCD) indicated a quadratic relationship with $p < 0.0001$ for adsorption capacity at saturation (q_s) and fraction of bed utilization (FBU). The results of the experiments performed under the optimized conditions, pH = 5.07, $C_0 = 137.86$ mg L^{-1}, $H = 2.99$ cm and $Q = 1.038$ mL min^{-1}, showed a q_s value of 62.32 mg g^{-1} and FBU of 72.26%, with a deviation value of less than 0.05 from the predicted q_s and FBU values. The obtained breakthrough curves were fitted with four mathematical models, Thomas, Bohart–Adams, Yan and Yoon–Nelson, in order to determine the limiting step of the mass transfer of the atrazine adsorption onto the composite. A desorption study of the composite revealed the high reuse potential for MCHAC, thus, the prepared material could be used as a low-cost and efficient adsorbent for the decontamination of polluted wastewater.

1. Introduction

Benin Republic is one of the top cotton producers in West Africa, with more than 600 000 tons of cotton produced each year. To achieve this performance, large quantities of chemical fertilizers, pesticides and herbicides are imported each year and used for cotton farming. This practice has led to pollution of the aquatic environment by the residues of phytosanitary products.[1] Atrazine is one of the triazine herbicides that are very selective and widely used for weed control in cotton and cereal crops. Atrazine is persistent, non-biodegradable and its residues may accumulate in seeds, sediments, fishery products and may contaminate surface water and groundwater. Moreover, atrazine is also classified as a hazardous compound due to the negative impact it has on the aquatic environment and human health.[2,3] Thus, several methods such as photodegradation,[4] electrocatalytic processes,[5] oxidation processes,[6] membrane techniques,[7] biological treatments[8] and adsorption[9,10] are used for the removal of atrazine from polluted water. Among these methods, adsorption processes have become very attractive techniques because of their simplicity and low cost.[11,12]

Activated carbon, chitosan and their composites have mainly been used as adsorbents for organic pollutants and heavy metals in wastewater.[13–16] However, after the adsorption process, the separation of the adsorbent-loaded pollutants from the reaction medium by filtration is very difficult. Thus, in order to solve the problem, research has been focused on the development of new materials for this purpose, including magnetic nanoparticles.[17,18] Magnetite (Fe$_3$O$_4$) is a non-toxic material, both to human health and the environment. The use of magnetic-based adsorbents in wastewater treatment has received wide attention because magnetic nanoparticles are endowed with surface charges and can be easily separated from the reaction matrix using a magnet.[19] Thus, magnetic nanoparticles have been combined with other materials such as graphene oxide,[9,20,21] activated carbon[17,22,23] and chitosan[24] for the removal of heavy metals, dyes and pesticide residues from

[a]*Laboratoire de Chimie de l'Eau et de l'Environnement (LCEE), Ecole Normale Supérieure de Natitingou, Benin. E-mail: jacquesfatombi@yahoo.fr; Tel: +229-97895404*

[b]*Laboratoire d'Expertise et de Recherche en Chimie de l'Eau et de l'Environnement (LERCEE), UAC, Benin*

[c]*Centre d'Elaboration de Matériaux et d'Etudes Structurales, Université de Toulouse – UPS, 29 rue Jeanne Marvig, Cedex 4, 31055 Toulouse, BP 94347, France*

water. However, activated carbon and chitosan mainly used for their development are of commercial origin, meaning that they contribute towards an increase in the cost of water treatment. Thus, this study focuses on the preparation of a new and low-cost, magnetite/chitosan/activated carbon (MCHAC) composite material that could improve the removal of pesticide residues from aqueous solutions and also be easily separable from the reaction matrix after the adsorption process is complete. The composite was prepared *via* the coprecipitation of a $FeSO_4$ and $FeCl_3$ mixture, using activated carbon (AC) prepared from peanut shells, and chitosan (CH) extracted from local crab shells. The prepared composite was characterized using Fourier-transform infrared (FTIR) spectroscopy, X-ray diffraction and N_2 adsorption/desorption measurements. Then, the adsorption potential of MCHAC was investigated on atrazine under a fixed bed column system. The dynamics of the adsorption process were optimized by response surface methodology (RSM) coupled with central composite design (CCD) and the modeling of the breakthrough curves was performed using mathematical models.

2. Experimental

2.1. Preparation of the magnetite/chitosan/activated carbon (MCHAC)

The CH and AC used for the development of the MCHAC were produced from crab and peanut shells respectively. The activated carbon was prepared *via* chemical activation using H_3PO_4 (85%, Sigma-Aldrich) of peanut shells collected from the women's cooperative in Natitingou town (Benin) with an impregnation ratio (weight of H_3PO_4/weight of peanut shells) of 3 : 1. The chitosan was produced by the deacetylation of chitin extracted from local crab shells collected from markets in Porto-Novo town (Benin). The preparation process and the characteristics of the CH and AC were described in detail in previous work.[13]

The MCHAC composite was prepared according to the coprecipitation method reported by Danalioglu *et al.*[25] and Qu *et al.*[26] According to the method, a mixture of 0.175 mol of $FeSO_4 \cdot 7H_2O$ (98.50%, Klincent Mumbai) and 0.350 mol of $FeCl_3$ (97%, Klincent Mumbai) with $n_{(Fe^{2+})} : n_{(Fe^{3+})} = 1 : 2$ was dissolved in 100 mL of distilled water under stirring at 300 rpm for 2 h. Then, a solution of 2.5% (w/v) of chitosan was prepared by dissolving 5.0 g of chitosan in 250 mL of a 5% acetic acid solution under stirring for 6 h. After preparing, the chitosan solution was added to a solution of a mixture of (Fe^{2+}/Fe^{3+}). After 6 h of stirring at 300 rpm, 10 g of activated carbon was introduced into the system. The obtained suspension was shaken for 6 h and then, 10 mL of 8 M NH_4OH (28%, Sigma-Aldrich) solution was added dropwise. The measured pH of the resulting mixture was in the range of 11–12. Then, the suspension was stirred using a helix agitator at 100 rpm under hydrothermal treatment at 80 °C for 3 h. The formed precipitate was collected using a magnet and then washed several times with distilled water and finally using 250 mL of absolute ethanol (96%, Sigma-Aldrich). The obtained MCHAC composite was oven dried at 60 °C for 12 h, and then crushed and sieved (0.1 mm to 0.2 mm). The schematic process of the preparation of the MCHAC composite is shown in Fig. 1.
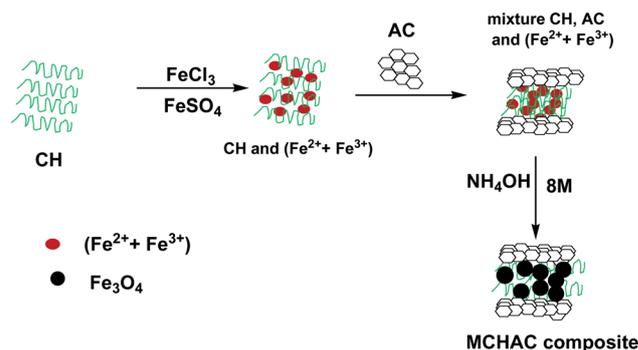

Fig. 1 Schematic overview of the preparation of MCHAC.

2.2. Atrazine solution

A stock solution of 500 mg L^{-1} of atrazine was prepared by dissolving 312.5 mg of atrazine (80%, Boachen Chemical Industry) in 500 mL of methanol (96%, Sigma-Aldrich). Atrazine solutions with concentrations ranging from 10 to 200 mg L^{-1} were prepared by diluting the stock solution with distilled water. The absorbance spectrum of the atrazine solution at 10 mg L^{-1} was recorded using a UV-Vis VWR 1600 spectrophotometer in order to determine the maximum absorption wavelength, which was determined to be 221 nm. After this, the calibration curve of atrazine solution (1–20 mg L^{-1}) was plotted and used to quantify the atrazine concentration in all of the experiments.

2.3. Characterization of the MCHAC composite

The MCHAC composite was characterized using different analytical methods. The point of zero-charge of the composite was determined according to the previously reported study by Marin *et al.*[27] FTIR spectroscopy was used to characterize the surface functional groups of MCHAC with a PerkinElmer 100 Series spectrometer. The X-ray diffraction of MCHAC was carried out using an analytical Empyrean X-ray diffractometer. The pore analysis of the composite was carried out using N_2 adsorption and desorption measurements at 77 K with a Micromeritics 2010 analyzer.

2.4. Fixed-bed column adsorption study

2.4.1. Fixed-bed experiments. The experiments were performed in glass columns with an internal diameter of 1.4 cm and a length of 50 cm. A fixed amount of glass wool was inserted at the bottom of the column to serve as the support material for the adsorbent. The atrazine solution of desired concentration was pumped into the column at a constant flow rate set to 1 mL min^{-1} using a peristaltic pump. The pH of the inlet atrazine solution was adjusted with HCl 0.1 M and NaOH 0.1 M. All tests were conducted at a room temperature of 30 °C. The volumes of the effluents of atrazine were collected at regular time intervals at the bottom of the column. The residual concentration of atrazine in the effluent samples was quantified using a UV-Vis VWR 1600 spectrophotometer at a wavelength of 221 nm. The pH (5 to 9), bed depth H (1 to 3 cm), flow rate Q (1 to 3 mL min^{-1}) and initial concentration of atrazine solution C_0 (40

Table 1 Characteristics of the experimental variables

Variables	Symbol	Values	
		Min.	Max.
pH	A	5	9
C_0 (mg L^{-1})	B	42.17	187.98
H (cm)	C	1	3
Q (mL min^{-1})	D	1	3

to 200 mg L^{-1}) were investigated in terms of the effect they have on the adsorption process. Breakthrough curves were obtained by continuous monitoring of the process. For this purpose, the breakthrough time (t_b), breakthrough concentration (C_b), saturation time (t_s), saturation concentration (C_s), adsorption capacity at the saturation time (q_s), and the fraction of bed utilization (FBU) can be expressed as follows:[28]

$$C_b = \frac{5 \times C_0}{100} \tag{1}$$

$$C_s = \frac{95 \times C_0}{100} \tag{2}$$

$$m_s = \frac{Q}{1000} \int_0^{t_s} (C_0 - C_s) \tag{3}$$

$$m_b = \frac{Q}{1000} \int_0^{t_b} (C_0 - C_b) \tag{4}$$

$$q_s = \frac{m_s}{w} \tag{5}$$

$$q_b = \frac{m_b}{w} \tag{6}$$

$$\text{FBU} = \frac{q_b}{q_s} \times 100 \tag{7}$$

where t_b and t_s (min) are the times taken to reach 5% and 95% of C_0 respectively, where C_0 (mg L^{-1}) is the initial concentration of atrazine solution, m_b and m_s (mg) are the weights of atrazine at breakthrough and saturation, respectively, w (g) is the weight of the composite bed in the column.

2.4.2. RSM-CCD optimization. RSM coupled with CCD was used to evaluate the individual as well as the combined effect of the independent variables that influence the adsorption of atrazine onto the MCHAC composite. Four independent variables, the C_0 (initial concentration of atrazine), pH of the atrazine solution, H (bed depth of the composite in the column), and Q (flow rate of the solution) were included in the RSM-CCD measurements. The experimental ranges of the four parameters were selected after the preliminary experiments. Their values with units and symbols are given in Table 1. In this study, the Design Expert version 11 software was used to model the adsorption capacity at equilibrium (q_s) and the FBU. The results obtained for twenty-four experiments as well as the responses predicted by the Design Expert software and using RSM-CCD are summarized in Table 2.

The quadratic polynomial model that links the responses q_s and FBU as a function of independent parameters was established using the following relationship:

$$Y = a_0 + \sum_{i=1}^{n} a_i X_i + \sum_{i=1}^{n} a_{ii} X_i^2 + \sum_{i=1}^{n-1} \sum_{j=i+1}^{n} a_{ij} X_i X_j + \varepsilon \tag{E1}$$

Table 2 Experimental data and predicted responses

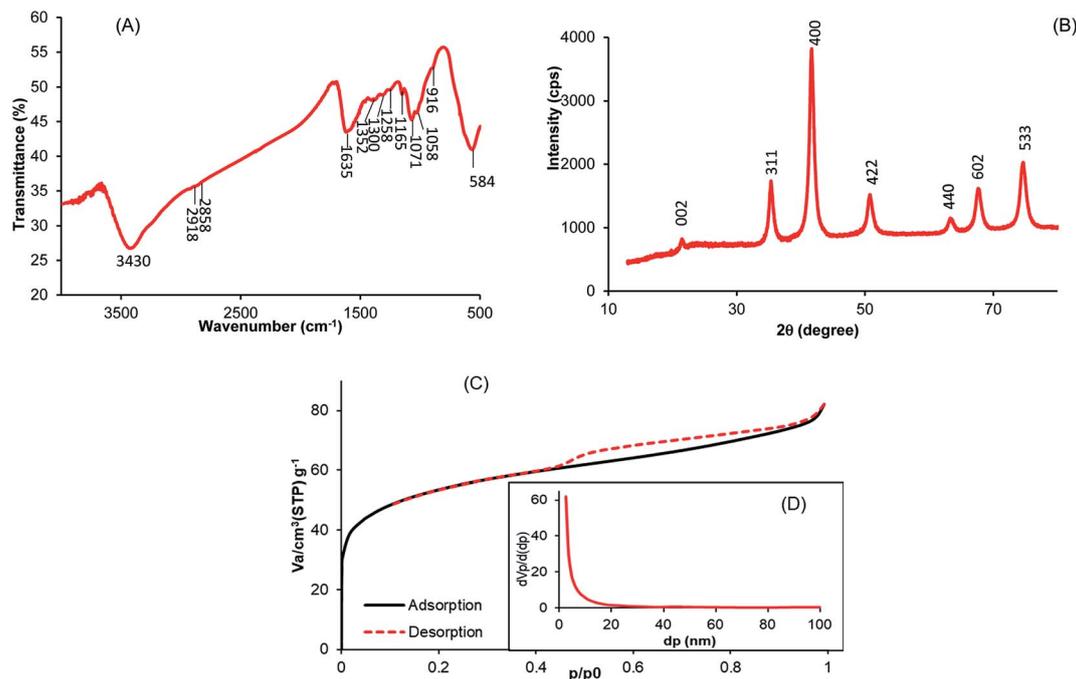| Run	Factor 1: A, pH	Factor 2: B, C_0 (mg L^{-1})	Factor 3: C, H (cm)	Factor 4: D, Q (mL min^{-1})	Response 1, q_s (mg g^{-1})	Predicted 1, (mg g^{-1})	Response 2, FBU (%)	Predicted 2, (%)
1	5	50.58	1	1	14.85	12.54	29.75	31.99
2	5	94.49	1	1	31.50	31.17	17.70	13.80
3	5	187.98	1	1	53.38	53.41	7.72	6.76
4	9	96.88	1	1	16.28	17.56	28.06	25.10
5	9	183.26	1	1	23.33	23.01	14.56	16.00
6	9	47.65	2	1	12.50	12.32	49.60	47.52
7	5	47.65	1	1	19.30	17.79	19.84	19.48
8	5	42.17	2	1	30.90	28.89	43.79	47.00
9	5	92.75	2	1	39.63	42.11	45.19	44.82
10	9	94.89	2	1	14.31	16.25	40.24	44.19
11	9	183.26	2	1	19.92	19.50	44.50	41.92
12	7	47.65	1	1	5.81	9.50	25.92	28.68
13	5	47.65	3	1	38.49	41.22	67.71	65.02
14	7	94.15	1	1	16.86	18.72	22.34	22.36
15	7	183.26	1	1	34.43	32.24	12.47	14.20
16	5	94.49	3	1	55.48	52.08	70.09	66.85
17	7	42.17	2	1	16.75	14.85	55.83	50.21
18	7	94.89	2	1	29.07	23.96	52.59	47.19
19	7	183.26	2	1	31.98	34.97	45.64	46.20
20	7	50.03	3	1	18.81	20.85	58.63	62.08
21	7	94.89	3	1	28.64	27.27	60.74	63.23
22	5	96.68	2	2	42.77	43.06	42.01	44.72
23	5	93.60	2	2	41.54	42.31	41.24	44.79
24	5	96.68	2	3	41.91	43.06	42.65	44.72

Fig. 2 (A) IRFT spectrum of MCHAC; (B) XRD pattern of MCHAC; (C) N$_2$ adsorption/desorption onto MCHAC; (D) pore distribution of MCHAC.

where Y is the predicted response; a_0, a_i, a_{ii} and a_{ij} are the constant, linear, quadratic and interaction values of regression coefficients, respectively; X_i and X_j are the coded variables; i and j are the coded independent parameters; and ε and n are the residual term and the number of variables, respectively.[29]

2.4.3. Modeling of the breakthrough curves. The shape of the breakthrough curves is an essential characteristic for the description of the adsorption dynamics. In order to model the breakthrough curves well, four mathematical models, Thomas,[30] Bohart–Adams,[31] Yoon–Nelson[32] and Yan,[33] were tested. The equations of these models can be expressed as follows:

Thomas:

$$\frac{C_t}{C_0} = \frac{1}{1 + \exp\left(\left(\frac{k_{Th}q_{Th}W}{Q}\right) - k_{Th}C_0 t\right)} \tag{8}$$

Bohart–Adams:

$$\frac{C_t}{C_0} = \frac{\exp(k_{BA}C_0 t)}{\exp\left(\frac{k_{BA}N_0 H}{F}\right) - 1 + \exp(k_{BA}C_0 t)} \tag{9}$$

Yoon–Nelson:

$$\frac{C_t}{C_0} = \frac{1}{1 + \exp(k_{YN}(t - \tau))} \tag{10}$$

Yan:

$$\frac{C_t}{C_0} = 1 - \frac{1}{1 + \left(\frac{C_0 Q t}{q_Y W}\right)^{a_Y}} \tag{11}$$

where k_{Th} (mL min^{-1} mg^{-1}) and q_{Th} (mg g^{-1}) are the kinetic rate and the adsorption capacity of the Thomas model, k_{BA} (mL min^{-1} mg^{-1}) is the kinetic rate of the Bohart–Adams model, N_0 (mg L^{-1}) is the saturation concentration, F (cm min^{-1}) is the linear rate of the solution ($F = Q/A$), A (cm^2) is the section area of the column $\left(A = \frac{\pi \times d^2}{4}\right)$ d (cm) is the internal diameter of the column, q_Y (mg g^{-1}) and a_Y (mL min^{-1} mg^{-1}) are the adsorption capacity and the rate constant of the Yan model, respectively, k_{YN} (min^{-1}) is the rate constant of the Yoon–Nelson model and τ (min) is the time taken to reach 50% of C_0.

2.5. Desorption and regeneration study

Column regeneration tests were performed by eluting the saturated bed with desorbing agents such as 0.10 M NaOH and 0.10 M HCl at a constant flow rate of 2 mL min^{-1} until a residual concentration of atrazine was less than 5% of C_0. The regenerated bed was then rinsed several times with distilled water at 2 mL min^{-1} for 1 h and then reused for the next adsorption/desorption cycle three times.

Table 3 Textural parameters of AC, CH, Fe$_3$O$_4$ and MCHAC

	Specific surface area (m^2 g^{-1})	Total volume of pore (cm^3 g^{-1})	Mean diameter of pore (nm)
AC	458.22	0.230	2.42
CH	0.14	0.0293	831.29
Fe$_3$O$_4$	100	0.297	11.86
MCHAC	189.50	0.126	2.66

RSC Advances

Table 4 ANOVA factors for q_s

Source	Sum of squares	df	Mean square	F value	P value
Model	3939.47	10	393.95	47.53	<0.0001
A-pH	76.41	1	76.41	9.22	0.0096
B-concentration	297.04	1	297.04	35.84	<0.0001
C-bed depth	121.94	1	121.94	14.71	0.0021
D-flow rate	3.61	1	3.61	0.4359	0.5206
AB	232.50	1	232.50	28.05	0.0001
AC	176.62	1	176.62	21.31	0.0005
AD	0.000	0			
BC	11.44	1	11.44	1.38	0.2612
CD	0.000	0			
A^2	138.07	1	138.07	16.66	0.0013
B^2	13.01	1	13.01	1.57	0.2324
C^2	6.23	1	0.7516	0.4017	
Residual	107.75	13	8.29		
Cor. total	4047.22	23			
Std dev.	2.88	R^2	0.9734	$R_{pred}{}^2$	0.9122
Mean	28.28	$R_{adj}{}^2$	0.9529	Adeq Precision	22.6957
CV	10.18				

2.6. Statistical analysis

The reliability of the fitting of the experimental data to the models was checked using the values of the coefficient of determination (R^2), the sum of the square errors (SSE) and the Chi-squared test (χ^2). A high R^2 value and low values for SSE and χ^2 reveal a good fit between the experimental and calculated data. R^2, SSE and χ^2 are expressed using the following relationships:[34]

$$R^2 = \frac{\sum_i^n \left(q_{i_{exp}} - \overline{q_{exp}}\right)^2 - \sum_i^n \left(q_{i_{exp}} - q_{i_{mod}}\right)^2}{\sum_i^n \left(q_{i_{exp}} - \overline{q_{exp}}\right)^2} \tag{12}$$

$$SSE = \sum_i^n \left(q_{e_{exp}} - q_{e_{mod}}\right)^2 \tag{13}$$

$$\chi^2 = \sum_i^n \frac{\left(q_{e_{exp}} - q_{e_{mod}}\right)^2}{q_{e_{mod}}} \tag{14}$$

where $q_{e_{exp}}$ and $q_{e_{mod}}$ (mg g^{-1}) are the experimental and calculated adsorption capacities from the model equation.

3. Results and discussion

3.1. Characteristics of MCHAC

The FTIR spectrum of the MCHAC composite is shown in Fig. 2A. The spectrum reveals a broad band near 3430 cm^{-1},

Table 5 ANOVA factors for the FBU

Source	Sum of squares	df	Mean square	F value	P value
Model	6981.44	10	698.14	54.45	<0.0001
A-pH	15.25	1	15.25	1.19	0.2953
B-concentration	12.03	1	12.03	0.9384	0.3504
C-bed depth	1950.53	1	1950.53	152.13	<0.0001
D-flow rate	34.50	1	34.50	2.69	0.1249
AB	8.80	1	8.80	0.6865	0.4223
AC	189.17	1	189.17	14.75	0.0020
AD	0.000	0			
BC	91.21	1	91.21	7.11	0.0194
CD	0.000	0			
A^2	26.58	1	26.58	2.07	0.1736
B^2	1.28	1	1.28	0.0999	0.7570
C^2	117.05	1	117.05	9.13	0.0098
Residual	166.68	13	12.82		
Cor. total	7148.11	23			
Std dev.	3.58	R^2	0.9767	$R_{pred}{}^2$	0.9225
Mean	39.12	$R_{adj}{}^2$	0.9587	Adeq Précision	25.1229
CV	9.15				
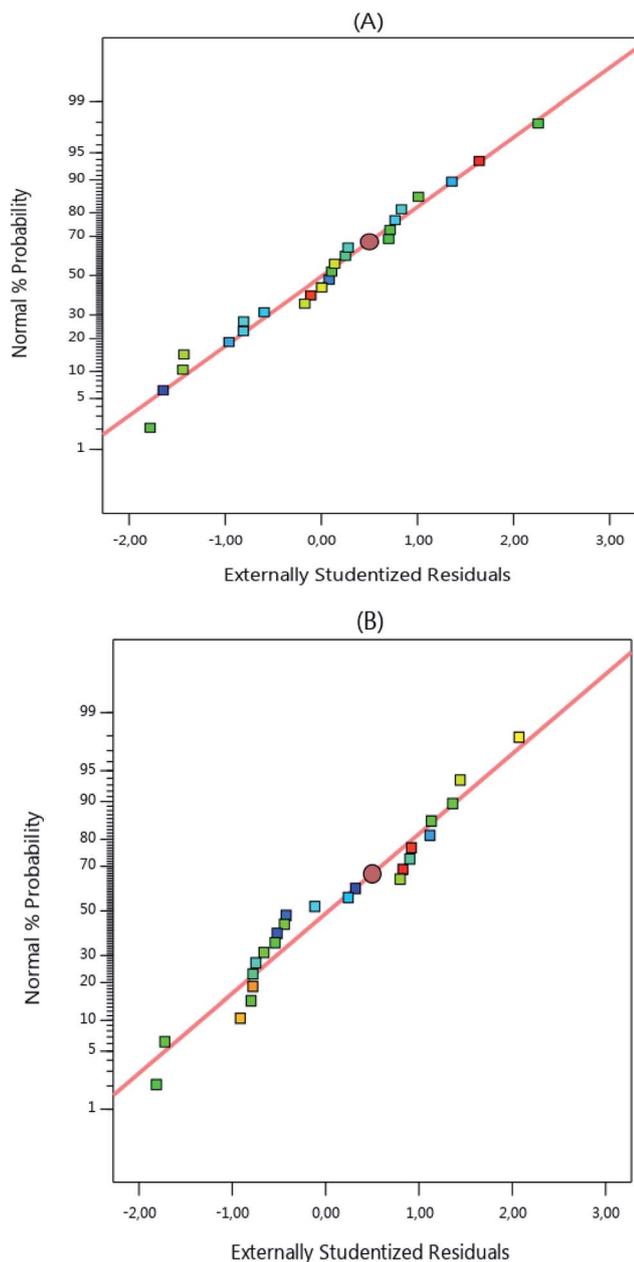
Fig. 3 Normal probability plots of the atrazine columns.

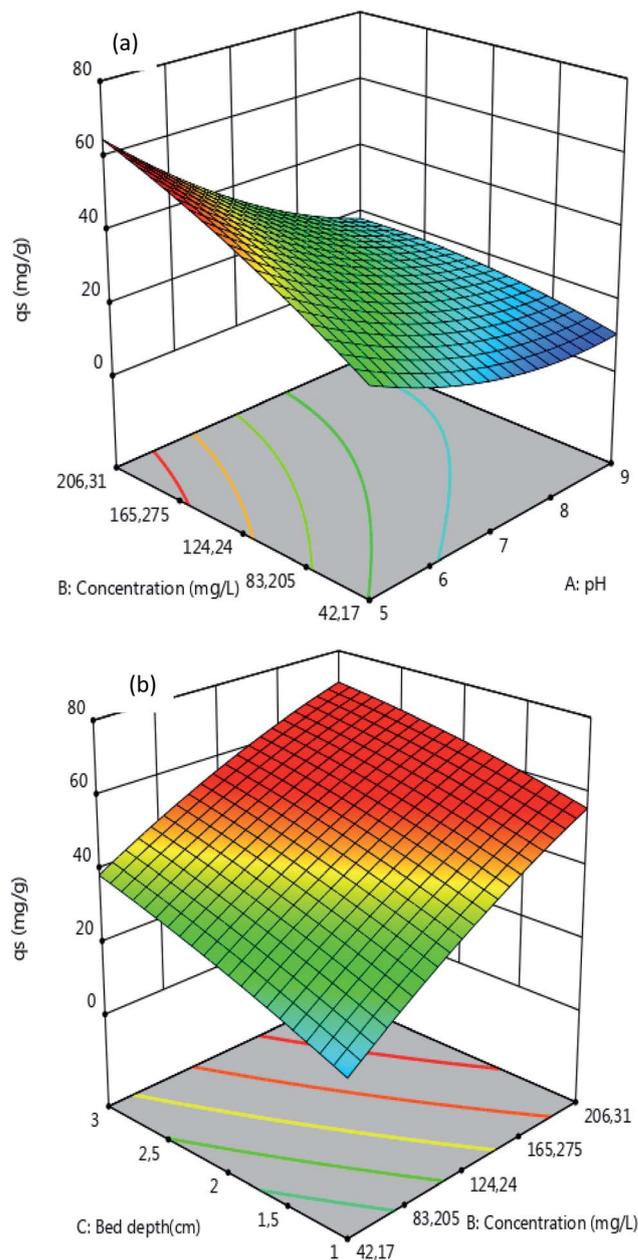Fig. 4 Response surfaces of q_s as function of the (a) initial concentration and pH ($H = 2$ cm, $Q = 2$ mL min^{-1}) and (b) bed depth and initial concentration (pH = 5, $Q = 2$ mL min^{-1}).

characterizing the stretching vibration of O–H from the composite structure.[21] The peaks observed at 2918 and 2858 cm^{-1} were assigned to the stretching vibration of C–H bonds from chitosan and activated carbon,[35,36] respectively. The band at 1635 cm^{-1} can be attributed to the vibration stretching of C=O in carbonyl groups.[25,37] The bands at 1352, 1165 and 1071 cm^{-1} can be assigned to the vibration stretching of C–N and the C–O–C bridge in chitosan.[38] In addition, the peak at 916 cm^{-1} may be attributed to the O–H bending vibration.[23] Finally, the intense band at 584 cm^{-1} was characteristic of the magnetic phase and was assigned to the stretching vibration of Fe–O bonds in the composite.[35,39] These observations suggested that magnetite, chitosan and activated carbon were successful combined in the MCHAC composite.

Fig. 2B shows the X-ray diffraction pattern of MCHAC, revealing that the composite has a crystalline structure with six characteristic peaks at $2\theta = 35.43°$, $41.70°$, $50.94°$, $63.70°$, $67.53°$ and $74.84°$, which can be attributed to the (311), (400), (422), (440), (602) and (533) planes of Fe$_3$O$_4$ (JCPDS no. 96-591-0064), respectively,[24,27,38,40] indicating the presence of magnetite in MCHAC. In addition, the diffraction peak with low intensity observed at $2\theta = 21.51°$ may be assigned to the (002) plane of the cellulose I structure in chitosan (JCPDS no. 03-0226).[13,15] The results also reveal that the peaks for activated carbon do not appear in the pattern of MCHAC because of the amorphous structure of the carbonaceous material.[17,36]
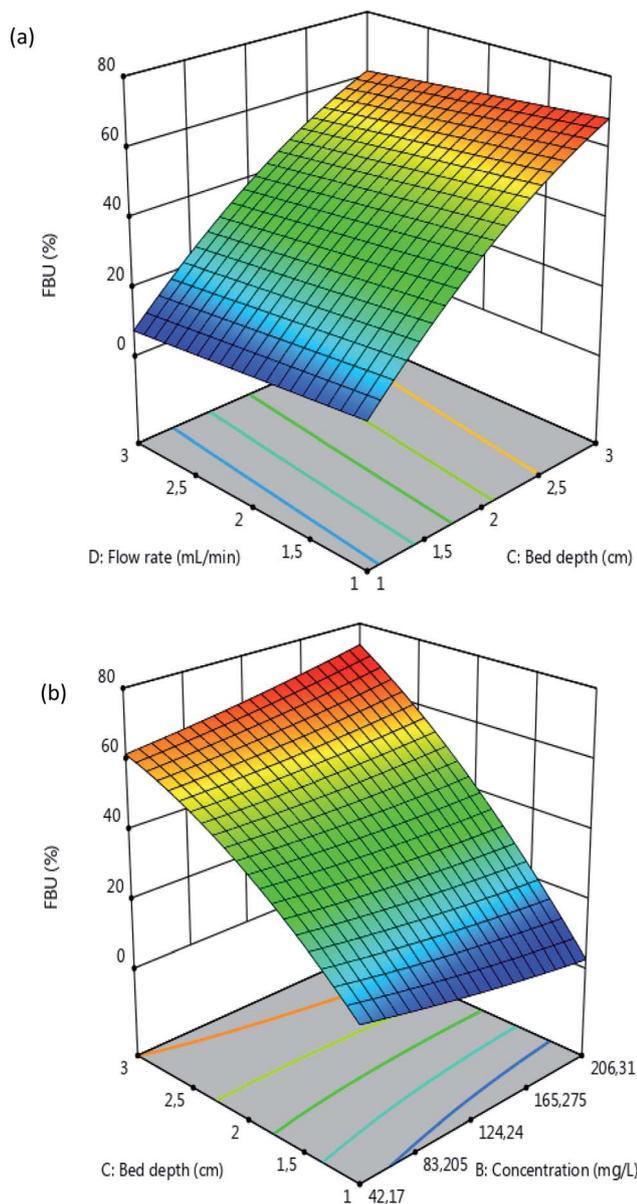
Fig. 5 Response surfaces of the FBU as a function of the (a) flow rate and bed depth (pH = 5, C_0 = 100 mg L^{-1}) and (b) bed depth and initial concentration (pH = 5, Q = 2 mL min^{-1}).

Fig. 6 Optimization of the conditions.

increasing the initial concentration C_0 of atrazine and the bed depth H, confirming that C_0 and H have a positive effect on q_s. The results also reveal that q_s decreases with an increase in the pH and the flow rate Q. The decrease in the q_s values with an increase in the pH may be justified by the progressive appearance of the negative loads on the adsorbent surface, which
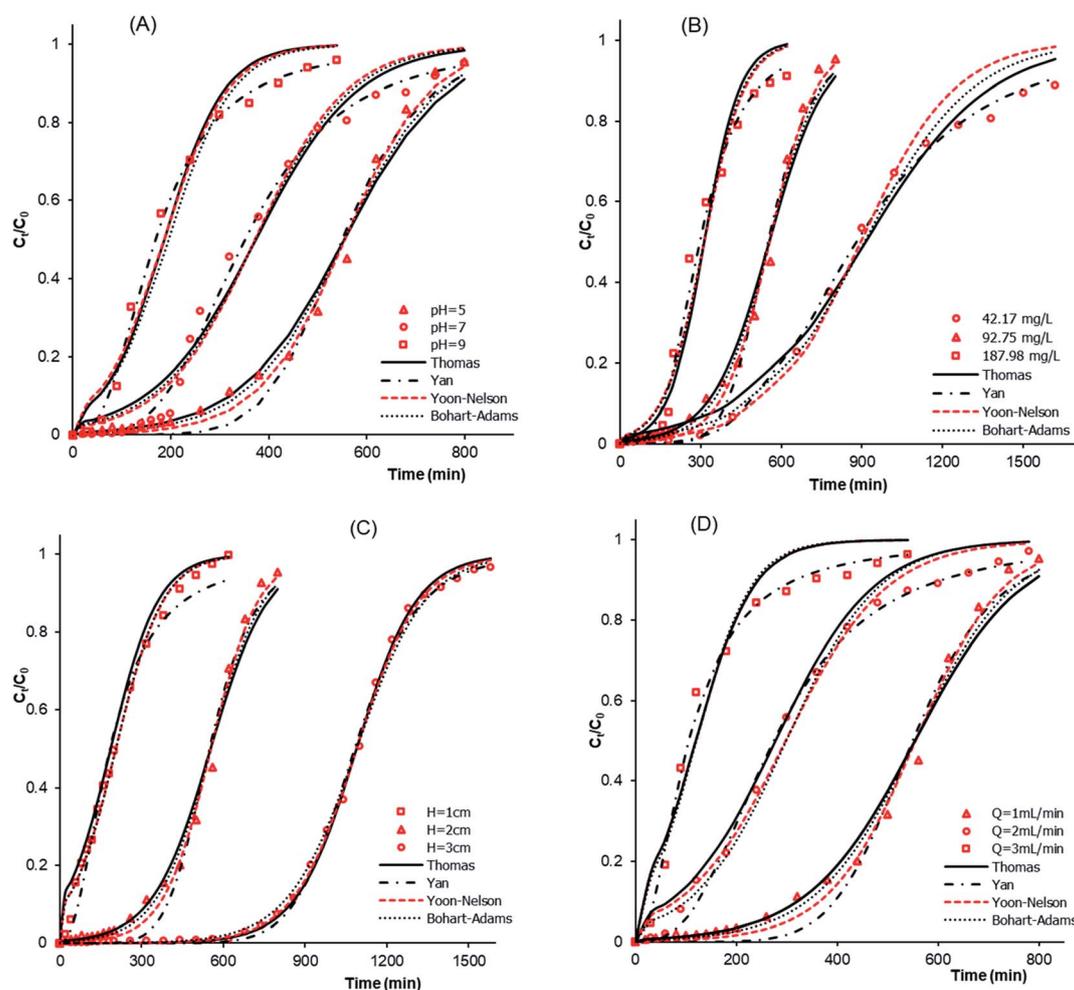
Fig. 7 Breakthrough curves and modeling showing the effects of the (A) pH of atrazine solution ($C_0 = 92.75$ mg L^{-1}, $Q = 1$ mL min^{-1}, $H = 2$ cm), (B) initial concentration of atrazine (pH = 5, $Q = 1$ mL min^{-1}, $H = 2$ cm), (C) bed height (pH = 5, $C_0 = 92.75$ mg L^{-1}, $Q = 1$ mL min^{-1}), and (D) flow rate (pH = 5, $C_0 = 92.75$ mg L^{-1}, $H = 2$ cm).

Table 6 Effects of the parameters on the breakthrough curves

Parameters	Atrazine solution pH			Initial concentration, C_0 (mg L^{-1})			Bed depth, H (cm)			Flow rate, Q (mL min^{-1})		
	5	7	9	42.17	92.75	187.98	1	2	3	1	2	3
t_b (min)	238	197	75	390	238	163	37	238	750	238	77	30
t_s (min)	800	800	540	1620	800	620	505	800	1510	800	730	508
q_b (mg g^{-1})	17.909	15.292	5.758	13.522	17.909	25.082	5.612	17.909	38.894	17.945	17.967	17.875
q_s (mg g^{-1})	39.632	29.074	14.309	30.900	39.632	47.049	31.704	39.632	55.484	39.630	42.77	41.910
FBU (%)	45.188	52.596	40.244	43.793	45.188	53.309	17.70	45.188	70.099	45.188	42.01	42.65

result in a low interaction between the adsorbent surface and the atrazine molecules, and a decrease in adsorption capacity. Indeed, the point of zero-charge (pHzpc) of MCHAC was found to be 6.8. In addition, atrazine is a weak base with a pKa value of 1.7.[42] Increasing the pH led to progressive deprotonation of the functional groups from the composite surface, and also suggested that the atrazine molecules were in the neutral form.[43] Moreover, an increase in the Q value led to an increase in the number of atrazine molecules ready to be adsorbed on the surface of adsorbent, which resulted in a decrease in the resistance to mass transfer through the adsorbent bed and reduced the residence time of adsorbate in the column to allow the diffusion of atrazine molecules into the pores of the adsorbent.

The results in Fig. 5 reveal that the FBU values increase with an increase in the bed depth and a decrease in the flow rate. It can also be seen that the FBU values increase with an increase in C_0 and the bed depth. These observations can be explained by the fact that at the beginning of the adsorption process with a low concentration of atrazine there is great availability of adsorbent surface for the adsorption to take place. Moreover, the increase in the bed depth led to the increase in the specific surface area of adsorbent, which provided more active sites available for adsorption and justified the increase in the FBU

values. In addition, the increase in the values of FBU with increasing in concentration of atrazine may be explained by the higher concentration gradient which occurred at a high initial concentration of atrazine, which then resulted in faster mass transfer through the bed depth of MCHAC.[44]

Furthermore, to optimize the experimental variables involved in the adsorption of atrazine, eqn (E2) and (E3) were used. The optimization parameters obtained are pH = 5.07, C_0 = 137.86 mg L^{-1}, H = 2.99 cm and Q = 1.038 mL min^{-1}, and the maximum response values q_s = 59.82 mg g^{-1} and FBU = 70.64% are displayed in Fig. 6. The experiments were carried out three times with similar conditions such as the optimized conditions, pH = 5.0, C_0 = 140 mg L^{-1}, H = 3 cm and Q = 1 mL min^{-1}, to give q_s = 62.32 ± 1.32 mg g^{-1} and FBU = 72.26 ± 2.04%, with deviation values of 0.042 for q_s and 0.045 for FBU of less than 0.05, suggesting good similarity between the observed responses and the results predicted by the model.

3.2.3. Effects of the parameters on the breakthrough curves

3.2.3.1 Effects of the solution pH and the initial concentration of atrazine. The effects of pH and of initial concentration were studied at pH 5, 7 and 9 and atrazine concentrations of 42.17, 92.75 and 187.98 mg L^{-1}. The results obtained at fixed values of a bed depth of H = 2 cm and flow rate of Q = 1 mL min^{-1} are

Table 7 Model parameters

	Parameters	Bed depth H (cm)			Initial concentration C_0 (mg L^{-1})			Atrazine solution pH			Flow rate Q (mL min^{-1})		
		1	2	3	42.17	92.75	187.98	5	7	9	1	2	3
	$q_{s_{exp}}$ (mg g^{-1})	31.699	39.632	55.485	30.900	39.632	47.050	39.632	29.074	14.309	39.632	42.77	41.91
Thomas	k_{Th} (mL min^{-1} mg^{-1})	0.122	0.101	0.096	0.101	0.101	0.081	0.101	0.101	0.173	0.101	0.104	0.184
	q_{Th} (mg g^{-1})	29.470	42.844	57.137	32.375	42.844	49.032	42.844	29.545	14.728	42.844	46.948	29.951
	R^2	0.997	0.995	0.997	0.995	0.995	0.986	0.995	0.992	0.990	0.995	0.997	0.982
	SSE	0.040	0.026	0.050	0.028	0.026	0.169	0.026	0.070	0.047	0.026	0.024	0.068
Yan	a_Y (mL min^{-1} mg^{-1})	2.203	6.641	9.436	3.730	6.641	3.647	6.641	3.489	2.585	6.641	2.770	2.022
	q_Y (mg g^{-1})	29.061	42.500	56.756	31.177	42.500	46.430	42.500	27.763	13.333	42.500	44.151	25.767
	R^2	0.994	0.995	0.999	0.999	0.995	0.996	0.995	0.998	0.999	0.995	0.998	0.997
	SSE	0.030	0.033	0.007	0.005	0.033	0.020	0.033	0.017	0.005	0.033	0.0077	0.009
Yoon–Nelson	k_{YN} (min^{-1})	0.011	0.012	0.009	0.006	0.012	0.013	0.012	0.011	0.015	0.012	0.010	0.018
	τ (min)	206.202	555.475	1088.380	896.104	555.475	312.988	555.475	371.752	186.249	555.475	297.562	119.778
	R^2	0.996	0.997	1.000	0.996	0.997	0.989	0.997	0.992	0.990	0.997	0.996	0.983
	SSE	0.017	0.014	0.005	0.053	0.014	0.065	0.014	0.069	0.046	0.014	0.023	0.067
Bohart–Adams	k_{BA} (mL min^{-1} mg^{-1})	0.123	0.110	0.084	0.117	0.110	0.073	0.110	0.108	0.163	0.110	0.114	0.194
	No (mg L^{-1})	15.820	20.200	26.917	15.222	20.200	23.074	20.200	13.970	7.378	20.200	22.951	14.359
	R^2	0.996	0.997	0.994	0.996	0.997	0.989	0.997	0.992	0.987	0.997	0.996	0.984
	SSE	0.018	0.018	0.008	0.035	0.018	0.065	0.018	0.070	0.050	0.018	0.026	0.068

shown in Fig. 7A, B and Table 6. The results depict a decrease in breakthrough time t_b, saturation time t_s, adsorption capacity at breakthrough q_b, adsorption capacity at saturation q_s and FBU, suggesting that increasing the pH results in a decrease in the adsorption efficiency of atrazine. In addition, it was revealed from Fig. 7B that t_b and t_s sharply decrease from 390 to 163 min and from 1620 to 620 min, respectively, with an increase in the atrazine concentration from 42.17 to 187.98 mg L^{-1} (Table 6). Finally, gradual increases in q_b, q_s and FBU were also observed upon increasing the atrazine concentration. Similar results were reported by Homem, and Wernke et al.,[44,45] in their studies on the adsorption of atrazine and diuron in a fixed-bed column.

3.2.3.2.   Effects of the bed depth and the flow rate. The effects that the bed depth and flow rate have on the adsorption process were investigated with H values of 1, 2 and 3 cm and Q in the range of 1–3 mL min^{-1}. The results obtained for pH = 5 and C_0 = 92.75 mg L^{-1} are shown in Fig. 7C and D. The results from Fig. 7C show that the t_b, t_s, q_b, q_s and FBU values increase with an increase in the bed depth. An increase in the bed depth values led to an increase in the number of available sites on the adsorbent surface, which resulted in significant mass transfer through the adsorbent bed and thus, justified the increase in q_b and q_s. The increase in t_b and t_s may be justified by the great resistance to transfer caused by an increase in the bed depth. Lonappan, and Batra et al.,[28,46] observed the same trend during the adsorption of diclofenac and bisphenol A in a fixed-bed column. The results presented in Fig. 7D indicate that, t_b and t_s decrease with an increase in the flow rate. This trend is due to the resistance to mass transfer through the adsorbent bed. In addition, the increase in q_s from 39.63 to 41.91 mg g^{-1} with an increase in the flow rate from 1 to 3 mL min^{-1} may be due to the decrease in mass transfer resistance. This behavior is in accordance with that noted by Hethnawi et al.[47] during the adsorption process of metformin.

3.2.4.   Dynamic modeling of breakthrough curves. To better describe the dynamic behavior of the adsorption process, the Thomas, Yan, Yoon–Nelson and Bohart–Adams mathematical models were used to fit the breakthrough curves. The results of the fitting and the calculated parameters are displayed in Fig. 7 and Table 7. All of the breakthrough curves are asymmetrical S-shaped curves, suggesting that the breakthrough curves are composed of two parts corresponding to two different mechanisms of the adsorption process.[48] The results of the fitting reveal that the Thomas model is a good fit to the experimental data. Moreover, the adsorption capacity q_{Th} values calculated using the Thomas model are slightly higher than the experimental q_s values. In addition, the values of the Thomas parameter k_{Th} increased with an increase in pH and Q values and then decreased with an increase in H and C_0. This observation implies that the adsorption mechanism is not controlled by the mass transfer at the interface of the adsorbent.[49] Furthermore, the Yan model showed a better fit to the experimental results because the R^2 values are close to 1 and the SSE values are too low. In addition, the adsorption capacity q_Y values calculated according to the Yan equation are close to the q_s values. Moreover, the values of the time τ taken to reach 50% of C_0 calculated according to the Yoon–Nelson model increased

with an increase in the bed depth and decreased with increases in pH, C_0 and flow rate (Table 7). Finally, the Bohart–Adams model reveals the highest R^2 values and lowest SSE values. This observation also shows that the Bohart–Adams model is a good fit to the experimental results. Therefore, surface diffusion was determined as the rate-limiting step of the adsorption process.[50] The values of the maximum volumetric capacity N_0 increased with an increase in the bed depth and C_0, and then decreased with an increase in flow rate and pH. The results of this study suggest that all of the models tested can be used to describe the adsorption dynamics of the adsorption of atrazine onto MCHAC.
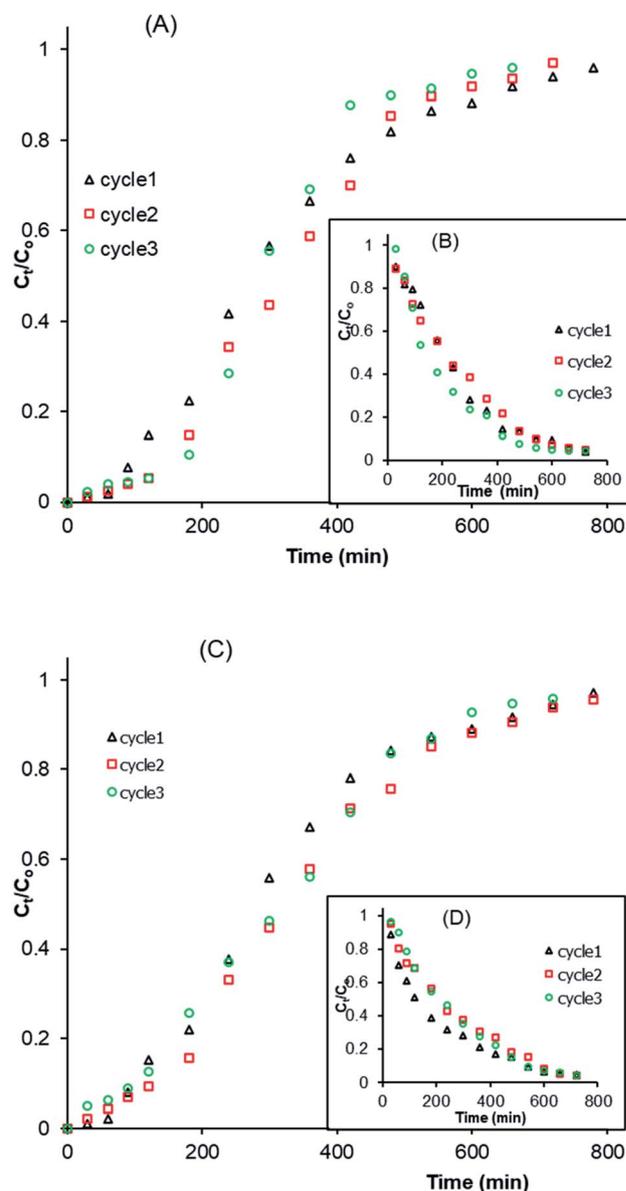

Fig. 8 Breakthrough curves of the adsorption/desorption of atrazine in a fixed-bed column by MCHAC over three cycles: (A and B) HCl; (C and D) NaOH; (A and C) adsorption; (B and D) desorption (C_0 = 96.68 mg L^{-1}, Q = 2 mL min^{-1}, H = 2 cm).

Table 8 Fixed-bed column adsorption process parameters for three adsorption/desorption cycles

		Desorbing agents	
	Parameters	HCl	NaOH
Cycle 1	t_s (min)	730.00	730.00
	q_s (mg g^{-1})	42.77	42.77
	FBU (%)	42.01	42.01
Cycle 2	t_s (min)	685.00	760.00
	q_s (mg g^{-1})	49.64	51.79
	FBU (%)	44.97	42.29
Cycle 3	t_s (min)	610.00	675.00
	q_s (mg g^{-1})	43.54	45.99
	FBU (%)	45.77	43.67

3.2.5. Desorption and regeneration study. The study of the adsorption and desorption of MCHAC was performed in order to determine the applicability and cost-effectiveness of the composite for use in water treatment applications. The columns were regenerated over three cycles using 0.1 M NaOH and 0.1 M HCl solutions as desorbing agents and the breakthrough curves of the regeneration process are displayed in Fig. 8. The results reveal the same trend with slight changes, suggesting that the composite can be regenerated over the three cycles tested. Furthermore, the results in Table 8 indicate a decrease in the saturation time t_s from 730 to 610 min with HCl and from 730 to 675 min with NaOH. In addition, a slight increase in the q_s and FBU values was noted during the process. The q_s values increased from 42.77 to 43.54 mg g^{-1} with HCl and from 42.77 to 45.99 mg g^{-1} with NaOH. The higher desorption efficiency of the composite with HCl and NaOH suggests the existence of a high affinity between the desorbing agents and the adsorbed atrazine molecules. In addition, the desorption results shown in Fig. 8B and D reveal a decrease in the contact time of the desorption with HCl (Fig. 8B) and an increase in the contact time of the desorption with NaOH (Fig. 8D). These observations suggest that the use of HCl solution as a column eluent could lead to a partial dissolution of the composite material during the desorption process. However, a significant difference is not observed between the weight of the composite material before and after the three adsorption/desorption cycles attempted, hence, the prepared composite has good recovery efficiency and its use for the treatment of contaminated wastewater would contribute to a significant reduction in the cost of the process. These results are in accordance with those reported by Homem et al.[45] and Ali et al.,[51] who studied the efficiency of atrazine desorption from *Moringa oleifera* seed husks and an iron nano-composite material.

4. Conclusion

A magnetite/chitosan/activated carbon composite was successfully prepared for the removal of the herbicide atrazine from aqueous solutions in a fixed-bed column system. The characteristics of MCHAC were measured using FTIR spectroscopy, XRD and BET analysis. The results reveal that the prepared material has a crystalline structure, mesoporous surface and a high specific surface area of 189.50 m^2 g^{-1}. The results from the RSM-CCD study reveal a value of $P < 0.0001$ for q_s and the FBU. The results also reveal that the MCHAC composite has good adsorption potential for atrazine in aqueous solution with a q_s value of 62.32 mg g^{-1} and an FBU value of 72.26%, obtained under the optimal conditions of pH = 5.07, an initial concentration of atrazine of $C_0 = 137.86$ mg L^{-1}, bed depth $H = 2.99$ cm and flow rate $Q = 1.038$ mL min^{-1}. The study of the breakthrough curves modeling suggested that the Bohart–Adams model gave the best fit to the experimental results, with the highest values of R^2 and lowest values of SSE. Accordingly, internal and external diffusion of atrazine molecules in the pores of the composite material was found to be the rate-limiting step of the mechanism of the adsorption process. After three cycles of adsorption/desorption, the breakthrough curves revealed the same trend. Overall, the magnetite/chitosan/activated carbon composite shows high adsorption of atrazine from aqueous medium, and high potential for its reusability after three cycles, and can thus be used as a low-cost and efficient adsorbent for atrazine and the removal of other pollutants from contaminated wastewater.

Conflicts of interest

There are no conflicts to declare.

Acknowledgements

References

1 M. A. N. Gbaguidi, H. H. Soclo, Y. M. Issa, B. Fayomi, R. Dognon, A. Agagbe, C. Bonou, A. Youssao, L. F. Dovonou and A. Sanni, *Int. J. Biol. Chem. Sci.*, 2011, **5**, 1476–1490.

2 S. A. Abdulelah, K. G. Crile, A. Almouseli, S. Awali, A. Y. Tutwiler, E. A. Tien, V. J. Manzo, M. N. Hadeed and R. M. Belanger, *Chemosphere*, 2020, **239**, 124786.

3 C. Sun, Y. Xu, N. Hu, J. Ma, S. Sun, W. Cao, G. Klobucar, G. Hu and Y. Zhao, *Chemosphere*, 2020, **244**, 125514.

4 H. Atarodi and H. Faghihian, *J. Photochem. Photobiol., A*, 2019, **382**, 111892.

5 S. Komtchou, N. Delegan, A. Dirany, P. Drogui, D. Robert and M. A. El Khakani, *Catal. Today*, 2020, **340**, 323–333.

6 Y. Hong, J. Peng, X. Zhao, Y. Yan, B. Lai and G. Yao, *Chem. Eng. J.*, 2019, **370**, 354–363.

7 P. N. Chandra and K. Usha, *Mater. Today: Proc.*, 2020, DOI: 10.1016/j.matpr.2020.05.263.

8 I. A. Saleh, N. Zouari and M. A. Al-Ghouti, *Environ. Technol. Innov.*, 2020, **19**, 101026.

9 P. K. Boruah, B. Sharma, N. Hussain and M. R. Das, *Chemosphere*, 2017, **168**, 1058–1067.

10 A. D. N'Diaye, C. Boudokhane, M. Kankou and H. Dhaouadi, *Chem. Ecol.*, 2019, **35**(7), 678–692.

11 A. Mojiri, J. L. Zhou, B. Robinson, A. Ohashi, N. Ozaki, T. Kindaichi, H. Farraji and M. Vakili, *Chemosphere*, 2020, **253**, 126646.

12 Z. Anfar, H. A. Ahsaine, M. Zbair, A. Amedlous, A. A. El Fakir, A. Jada and N. El Alem, *Crit. Rev. Environ. Sci. Technol.*, 2019, **50**(10), 1043–1084.

13 J. K. Fatombi, E. A. Idohou, S. A. Osseni, I. Agani, D. Neumeyer, M. Verelst, R. Mauricot and T. Aminou, *Fibers Polym.*, 2019, **20**, 1820–1832.

14 J. K. Fatombi, I. Agani, S. A. Osseni, E. A. Idohou, D. Neumeyer, M. Verelst, R. Mauricot and T. Aminou, *Desalin. Water Treat.*, 2020, **189**, 250–263.

15 E. A. Idohou, J. K. Fatombi, S. A. Osseni, I. Agani, D. Neumeyer, M. Verelst, R. Mauricot and T. Aminou, *Surf. Interfaces*, 2020, **21**, 100741.

16 Z. Anfar, A. Amedlous, A. A. El Fakir, H. A. Ahsaine, M. Zbair, S. Lhanafi, R. El Haouti, A. Jada and N. El Alem, *ACS Omega*, 2019, **4**, 9434–9445.

17 Z. Anfar, A. Amedlous, A. A. El Fakir, M. Zbair, H. A. Ahsaine, A. Jada and N. El Alem, *Chemosphere*, 2019, **236**, 124351.

18 L. Spessato, A. L. Cazetta, S. Melo, O. Pezoti, J. Tami, A. Ronix, J. M. Fonseca, A. F. Martins, T. L. Silva and V. C. Almeida, *J. Mol. Liq.*, 2020, **300**, 112282.

19 F. Mashkoor and A. Nasar, *J. Magn. Magn. Mater.*, 2020, **500**, 166408.

20 R. Xing, J. He, P. Hao and W. Zhou, *Colloids Surf., A*, 2020, **589**, 124466.

21 M. A. Andrade, T. R. T. Santos, M. F. Silva, M. F. Vieira, R. Bergamasco and S. Hamoudi, *Sep. Sci. Technol.*, 2018, **54**(16), 2653–2670.

22 M. Y. Badi, A. Azari, H. Pasalari, A. Esrafili and M. Farzadkia, *J. Mol. Liq.*, 2018, **261**, 146–154.

23 C. S. Castro, M. C. Guerreiro, M. Gonc, L. O. A. Oliveira and A. S. Anastacio, *J. Hazard. Mater.*, 2009, **164**, 609–614.

24 H. Rasoulzadeh, M. H. Dehghani, A. S. Mohammadi, R. R. Karri, R. Nabizadeh, S. Nazmara, K. H. Kim and J. N. Sahu, *J. Mol. Liq.*, 2020, **297**, 111893.

25 S. T. Danalioglu, S. S. Bayazit, O. K. Kuyumcu and M. A. Salam, *J. Mol. Liq.*, 2017, **240**, 589–596.

26 S. Qu, J. Wang, J. Kong, P. Yang and G. Chen, *Talanta*, 2007, **71**, 1096–1102.

27 P. Marin, R. Bergamasco, A. N. Modenes, P. R. Paraiso and S. Hamoudi, *Process Saf. Environ. Prot.*, 2019, **123**, 59–71.

28 L. Lonappan, T. Rouissi, Y. Liu, S. K. Brar and R. Y. Surampalli, *J. Environ. Chem. Eng.*, 2019, **7**, 102894.

29 H. Mahdizadeh and M. Malakootian, *Process Saf. Environ. Prot.*, 2019, **123**, 299–308.

30 C. H. J. Thomas, *J. Am. Chem. Soc.*, 1944, **66**(2), 1664–1666.

31 G. S. Bohart and E. Q. Adams, *J. Franklin Inst.*, 1920, **189**(5), 669.

32 Y. H. Yoon and J. H. Nelson, *Am. Ind. Hyg. Assoc. J.*, 1984, **45**(8), 509–516.

33 G. Yan, T. Viraraghavan and M. Chen, *J. Franklin Inst.*, 2001, **19**(1), 25–43.

34 K. Y. Foo and B. H. Hameed, *Adv. Colloid Interface Sci.*, 2009, **149**, 19–27.

35 H. Karaer and I. Kaya, *Microporous Mesoporous Mater.*, 2016, **232**, 26–38.

36 F. C. Cavusoglu, S. Akan, E. A. Ari, E. Cetinkaya, E. Colak, G. N. Dastan, S. Deniz, D. Erdem, M. Koksal, S. Korkmaz, N. Onsekiz, B. Orucoglu, D. Ozkaya, H. B. Uslu, C. Unal, O. Yildiz, S. O. Aydinoglu and S. S. Bayazit, *Korean J. Chem. Eng.*, 2019, **36**(11), 1915–1921.

37 I. Agani, J. K. Fatombi, N. Topanou, E. A. Idohou and T. Aminou, *Am. J. Appl. Chem.*, 2020, **8**(3), 82–88.

38 T. Ahamad, M. Naushad and M. Alshahrani, *Int. J. Biol. Macromol.*, 2020, **147**, 258–267.

39 Z. Weijiang, Z. Yace, G. Yuvaraja and X. Jiao, *Int. J. Biol. Macromol.*, 2017, **105**, 422–430.

40 M. Malakootian, A. Nasiri and H. Mahdizadeh, *Water Sci. Technol.*, 2018, **78**(10), 2158–2170.

41 W. W. Tang, G. M. Zeng, J. L. Gong, Y. Liu, X. Y. Wang, Y. Y. Liu, Z. F. Liu, L. Chen, X. R. Zhang and D. Z. Tu, *Chem. Eng. J.*, 2012, **211–212**, 470–478.

42 L. F. Cusioli, C. O. Bezerra, H. B. Quesada, A. T. A. Baptista, L. Nishi, M. F. Vieira and R. Bergamasco, *Environ. Technol.*, 2019, DOI: 10.1080/09593330.2019.1653381.

43 M. Shirmardi, N. Alavi, E. C. Lima, A. Takdastan, A. H. Mahvi and A. A. Babaei, *Process Saf. Environ. Prot.*, 2016, **103**, 23–35.

44 G. Wernke, M. R. F. Klen, M. F. Vieira, P. Y. R. Suzaki, H. K. S. de Souza, Q. L. Shimabuku and R. Bergamasco, *Environ. Technol.*, 2018, **41**(5), 638–648.

45 N. C. Homem, A. M. S. Vieira, R. Bergamasco and M. F. Vieira, *Can. J. Chem. Eng.*, 2018, **9999**, 1–11.

46 S. Batra, D. Datta, S. N. Beesabathuni, N. Kanjolia and S. Saha, *Process Saf. Environ. Prot.*, 2019, **122**, 232–246.

47 A. Hethnawi, M. Alnajjar, A. D. Manasrah, A. Hassan, G. Vitale, R. Jeong and N. N. Nassar, *Colloids Surf., A*, 2020, **597**, 124814.

48 N. Blagojev, D. Kukic, V. Vasic, M. Sciban, J. Prodanovic and O. Bera, *J. Hazard. Mater.*, 2019, **363**, 366–375.

49 J. Lopez-Cervantes, D. I. Sanchez-Machado, R. G. Sanchez-Duarte and M. A. Correa-Murrieta, *Adsorpt. Sci. Technol.*, 2018, **36**(1–2), 215–232.

50 P. Liao, Z. Zhan, J. Dai, X. Wu, W. Zhang, K. Wang and S. Yuan, *Chem. Eng. J.*, 2013, **228**, 496–505.

51 I. Ali, Z. A. Al-Othman and A. Al-Warthan, *Int. J. Environ. Sci. Technol.*, 2016, **13**, 733–742.